



Phonon engineering of boron nitride via isotopic enrichment

Mingze He¹, Lucas Lindsay², Thomas E. Beechem³, Thomas Folland^{1,4}, Joseph Matson⁵, Kenji Watanabe⁶, Andrey Zavalin⁸, Akira Ueda⁸, Warren. E. Collins⁸, Takashi Taniguchi⁷, Joshua D. Caldwell^{1,a)} ^⑤

Received: 18 May 2021; accepted: 21 October 2021; published online: 9 November 2021

Phonon polaritons (PhPs) enable a variety of applications, yet it requires PhPs supported in the desired frequency range. The two BN allotropes (cubic and hexagonal, cBN and hBN) are of particular interest, as their optic phonons fall within the so-called molecular-fingerprint region (~ 1000–1610 cm⁻¹). However, there remains a spectral gap between PhPs covered by these two, limiting applications. Thus, we isotopically engineered hBN and cBN and examined the optic phonons. For hBN, enhancement of the optic phonon lifetimes and shifted frequencies are observed. However, lifetimes are observed to decrease with the enrichment of cBN by ¹⁰B, ¹¹B, and ¹⁵N. We propose that the reduced lifetimes are not due to intrinsic loss, but rather increased defect concentrations resulting from the modified growth, supported by first-principles calculations. Thus, reducing the extrinsic defects in isotopically engineered cBN may present a path toward overcoming these restrictions for applications in the molecular-fingerprint region.

Introduction

Due to the long free-space wavelengths associated with radiation in the infrared (IR) to terahertz spectral domains, the realization of flat and sub-diffractional optical components promise advances in imaging [1], communications [2], sensing [3] and thermal emitters [4]. Nanoscale photonic elements in the IR can be enabled through polaritons—quasiparticles composed of an oscillating charge and a photon—that allow the confinement of light to length-scales well below the diffraction limit [5, 6]. These polaritons are supported when materials exhibit a negative real part of the dielectric function, which occurs at frequencies below the plasma frequency for plasmon polaritons (PPs) or between the transverse (TO) and longitudinal (LO) optic phonons (the so-called Reststrahlen band, RB) for phonon polaritons (PhPs) [4]. As optic phonons exhibit much longer lifetimes than

free carriers, the optical losses of PhPs are significantly lower than their PP counterparts. This has been experimentally demonstrated by large quality factors reported for sub-diffractional optical antennas [7–13]. Benefitting from the low-loss, PhPs are of interest for use in molecular sensing via surface-enhanced IR absorption (SEIRA) and strong coupling [12, 14–16], where sensitivity to monolayers of chemically bonded species [16] has been demonstrated, as well as solid-state, narrow-band thermal emitters for IR optical sources [17–19]. However, all of these applications demand polar crystals supporting PhPs at the desired operational frequencies, while maintaining low optical loss. Boron nitride (BN) allotropes are particularly promising to this end, as their RBs overlap with much of the so-called "molecular-fingerprint" portion of the IR-spectral window containing a host of chemical vibrational bands [20].

¹Department of Mechanical Engineering, Vanderbilt University, Nashville, TN 37212, USA

²Materials Science and Technology Division, Oak Ridge National Laboratory, Oak Ridge, TN 37831, USA

³ Center for Integrated Nanotechnologies, Sandia National Laboratories, Albuquerque, NM 87185, USA

⁴ Department of Physics and Astronomy, The University of Iowa, Iowa City, IA 52242, USA

⁵ Interdisciplinary Materials Science Program, Vanderbilt University, Nashville, TN 37212, USA

⁶ Research Center for Functional Materials, National Institute for Materials Science, 1-1 Namiki, Tsukuba 305-0044, Japan

 $^{^{7}}$ International Center for Materials Nanoarchitectonics, National Institute for Materials Science, 1-1 Namiki, Tsukuba 305-0044, Japan

⁸ Center for Photonic Materials and Devices, Physics Department, Fisk University, Nashville, TN 37208, USA

^{a)}Address all correspondence to this author. e-mail: josh.caldwell@vanderbilt.edu



Recent work with hexagonal boron nitride (hBN) nanostructures, for instance, has demonstrated highly sensitive chemical sensing through strong coupling phenomena [12], while further efforts have highlighted the potential for lithography-free nanostructuring of cubic boron nitride (cBN) [20]. Spectrally, as shown in Fig. 1, the RB of natural hBN spans 1364-1614 cm⁻¹, whereas that of natural cBN extends from ~ 1050 to 1305 cm⁻¹. The two allotropes together cover much of the molecularfingerprint region (1050-1614 cm⁻¹) despite a conspicuous gap from ~ 1305-1364 cm⁻¹. One way to shrink the gap is to shift the RBs of the BN allotropes via isotopic enrichment, as has been recently demonstrated for hBN [4], where a 35 cm⁻¹ spectral shift in the TO phonons between monoisotopic h¹⁰BN and h¹¹BN (>99%) crystals was reported [4]. Isotopic enrichment also leads to lower optical loss due to reduced scattering from isotopic mass variations within the crystal [4]. Lower loss, in turn, leads to sharper PhP resonances, and opens new opportunities in planar metasurfaces [21, 22], reconfigurable on-chip photonics [23, 24], and improvements in hyperlens imaging [25]. However, the benefits of this approach have not been explored within cBN, which could further broaden the spectral range of BN-based RBs for a variety of nanophotonic applications.

In response, we explore the dependence of the optic phonon energies and lifetimes in isotopically engineered hBN and cBN crystals. Specifically, by comparing our data from isotopically enriched hBN grown by the high-pressure, high-temperature (HPHT) method [26] with that collected from similar hBN grown from molten-metal solutions [4], we show that similar improvements in phonon lifetimes are realized regardless of synthesis method. More importantly, we extend this methodology to realize ¹⁰B, ¹¹B, and ¹⁵N-enriched cBN, characterizing the

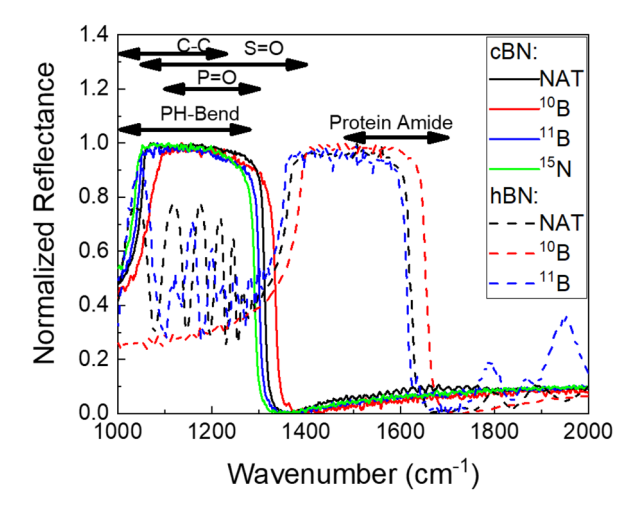


Figure 1: Reflectance data of different isotopically engineered cBN and hBN. The horizontal arrows represent the frequency ranges of some molecular vibrations. NAT designates natural isotope abundances.

phonon properties via both Raman and FTIR spectroscopies. Our results illustrate that significant spectral tuning is achieved via enrichment. Counterintuitively, measured phonon lifetimes in all isotopically engineered cBN are shorter than those measured in the naturally abundant cBN samples. This does not come from intrinsic anharmonic scatterings, but rather stems from higher extrinsic defect concentrations (i.e., impurities) within the enriched materials, as supported by observed crystal discoloration and first-principles calculations. These calculations predict a further two-fold improvement in the optic phonon lifetimes in isotopically enriched cBN with minimal extrinsic defects as observed in colorless, high-purity natural cBN crystals [27]. We then report the IR dielectric functions of different isotopically engineered cBN materials to enable devices employing these materials, for SEIRA spectroscopy and nanophotonic concepts in the IR.

Results and discussion

Modifying the isotopic concentration of a compound results in a net change in the atomic and crystal reduced mass and thus corresponding vibrational energies without altering chemical bonding. For hBN and cBN, due to the relatively light atomic mass of nitrogen and boron, even a 1 amu change in the mass can result in a \sim 3% change in frequency, and thus can induce a relatively large shift in the optic phonon dispersion. This is observed by tracking the spectral positions of the RBs as a function of isotope mass, where a lighter (heavier) isotope results in a RB with higher (lower) frequency (Fig. 1). With these spectral shifts, the gap between the RBs of cBN and hBN is reduced from \sim 60 cm $^{-1}$ in their naturally abundant forms to \sim 26 cm $^{-1}$ between c 10 BN and h 11 BN. As such, the combination of isotopically enriched cBN and hBN can cover a broad range of the molecular-fingerprint region, reaching from 1040 to 1650 cm $^{-1}$.

In addition to the spectral shifting of the phonon frequencies, isotopic enrichment also affects the zone-center phonon lifetimes indirectly by altering intrinsic anharmonic scattering channels and directly by reducing phonon-isotope scattering. This has been reported for hBN, where nearly monoisotopic h¹⁰BN and h¹¹BN were demonstrated to exhibit two- to threefold longer lifetimes [4, 28]. While first-principles calculations indicate the phonon lifetimes of monoisotopic hBN can be as high as 8 ps [4], the reported experimental data are limited to ~ 1.7 ps, which is presumed due to oxygen and carbon impurities [4]. Here, the hBN crystals are grown by a different method, i.e., HPHT [26], which may lead to different impurity types and concentrations and thus, scattering rates. To directly extract the phonon frequencies and lifetimes, we performed micro-Raman spectroscopy. As mentioned in previous studies [4], LO phonons within the upper RB of hBN are not Raman-active, and thus, we only probe the TO phonons



via this method. The TO phonon frequencies and full-width half maximums (FWHMs) are extracted by fitting the experimental line-shape to a Voigt distribution and then deconvolving the response function of the spectrometer using Posener's Tables to obtain the Lorentzian contribution stemming from the material. Using the energy-time uncertainty relation, the Lorentzian width is then used to calculate the phonon lifetime [29, 30]. More complete details on the Raman and FTIR experiments are provided in the Supplementary Information.

The TO phonon frequencies and lifetimes of our hBN synthesized by HPHT are tabulated in Table 1 and compared with data from Ref. [4], where phonon energies are nearly identical to the previous report [4]. We, therefore, assert that the isotope concentrations for the isotopically enriched hBN presented here are also over 99% purity. Consistent with previous reports, the isotopically enriched hBN samples exhibit improved phonon lifetimes compared with natural hBN. Further, the phonon lifetimes of HPHT grown hBN are longer than hBN grown via molten-metal solutions [4] (~20–35% improvements), indicating improved crystal quality, yet the phonon lifetime is still limited by impurities.

While hBN has been demonstrated as a promising material for several applications [31], including hyperlens imaging [1, 32, 33], quantum photonics [34-36] and as a deep-UV emitter [37-39], cBN offers additional opportunities as a high-quality material supporting PhPs within the spectral range of 1055 and 1305 cm⁻¹, which also corresponds to the molecular-fingerprint region of the electromagnetic spectrum (Fig. 1). To evaluate the material quality for such applications, we synthesized cBN crystals with different isotopic enrichments and spectrally characterized them using Raman and FTIR in a comparable way to the hBN. In cBN, the TO and LO phonons are observed in our backscattering Raman experiment (see Fig. 2a), allowing for a complete Raman characterization of the RB. The resulting phonon frequencies, FWHMs, and phonon lifetimes are provided in Table 2. Similar to the case of isotopically enriched hBN, the zone-center optical phonon frequencies of isotopically enriched cBN exhibit significant spectral shifts. However, isotopically engineered cBN samples exhibit shorter phonon lifetimes, contrary to expectations based on a reduction in isotopic mass variance.

To understand the influence of isotopic enrichment, we quantitatively determine the isotopic densities by examining the measured phonon frequency changes within a harmonic oscillator model. Mathematically, the model is written as

$$\sqrt{\frac{\mu}{g}} = \frac{1}{\omega} \tag{1}$$

where μ is the reduced mass, g a spring constant defined by the bond strength, and ω the vibration frequency. As the spring constant g is defined by chemical bond strength between atoms, we assume this to be independent of isotopic enrichment. Under this assumption, we calculate g based on measured phonon frequencies and reduced mass of naturally abundant cBN (11 B 80% and 15 N 99.99%). The isotopic concentrations of isotopically engineered cBN samples are then calculated based on their TO and LO frequencies, and the results are tabulated in Table 2. From these efforts, we approximate that the isotope concentrations for c^{11} BN and c^{15} N are > 99% and 98%, respectively, while for c^{10} BN is 88%.

For the nearly monoisotopic c¹¹BN samples (>99%), we expect a net increase in the phonon lifetime as phonon-isotope scattering decreases [4]; however, as stated above, reduced phonon lifetimes are observed. To assess intrinsic phonon properties of monoisotopic cBN, first-principles calculations are performed to deduce the phonon dispersion of pure c¹⁰BN, pure c¹¹BN, and natural cBN, as shown in Fig. 2(b). The dispersion was determined by diagonalization of the dynamical matrix:

$$D_{\alpha\beta}^{kk'}(\overrightarrow{q}) = \frac{1}{\sqrt{m_k m_{k'}}} \sum_{l'} \Phi_{\alpha\beta}^{0k,l'k'} e^{i\overrightarrow{q} \cdot \overrightarrow{R}_{l'}}$$
(2)

for phonon wavevector \overrightarrow{q} (for Raman measurements $\overrightarrow{q} \approx 0$), where m_k is the isotopically averaged mass of the kth atom, and \overrightarrow{R}_l is a lattice vector locating the lth unit cell. $\Phi_{\alpha\beta}^{[k,l'k']}$ are harmonic interatomic force constants linking atom lk and atom l'k' and calculated via density functional perturbation theory [40, 41]. As the isotopically averaged B mass decreases from 11 to 10 B, the optical branches are shifted to higher frequencies (Fig. 2b). The calculated TO and LO Raman-active phonon frequencies for natural cBN (ω_{TO} =1057 cm $^{-1}$, ω_{LO} =1285 cm $^{-1}$) and cBN with isotopically pure 10 B (ω_{TO} =1080 cm $^{-1}$, ω_{LO} =1314 cm $^{-1}$) agree well with measurements.

TABLE 1: Phonon properties of hBN extracted from Raman spectra. Peak positions and standard deviation (STD) are extracted from a series of measurements.

hBN	Peak [cm ⁻¹]	± Peak	FWHM [cm ⁻¹]	± FWHM [cm ⁻¹]	Lifetime [ps]
h ¹⁰ BN	1393.0	0.5	2.71	0.01	1.96
h ¹¹ BN	1357.0	0.5	2.36	0.01	2.24
Natural hBN	1365.8	0.5	7.22	0.01	0.73
h ¹⁰ BN [5]	1395.5	N/A	3.33	N/A	1.6
h ¹¹ BN [5]	1356.8	N/A	3.25	N/A	1.65
Natural hBN [5]	1365.6	N/A	8.34	N/A	0.7



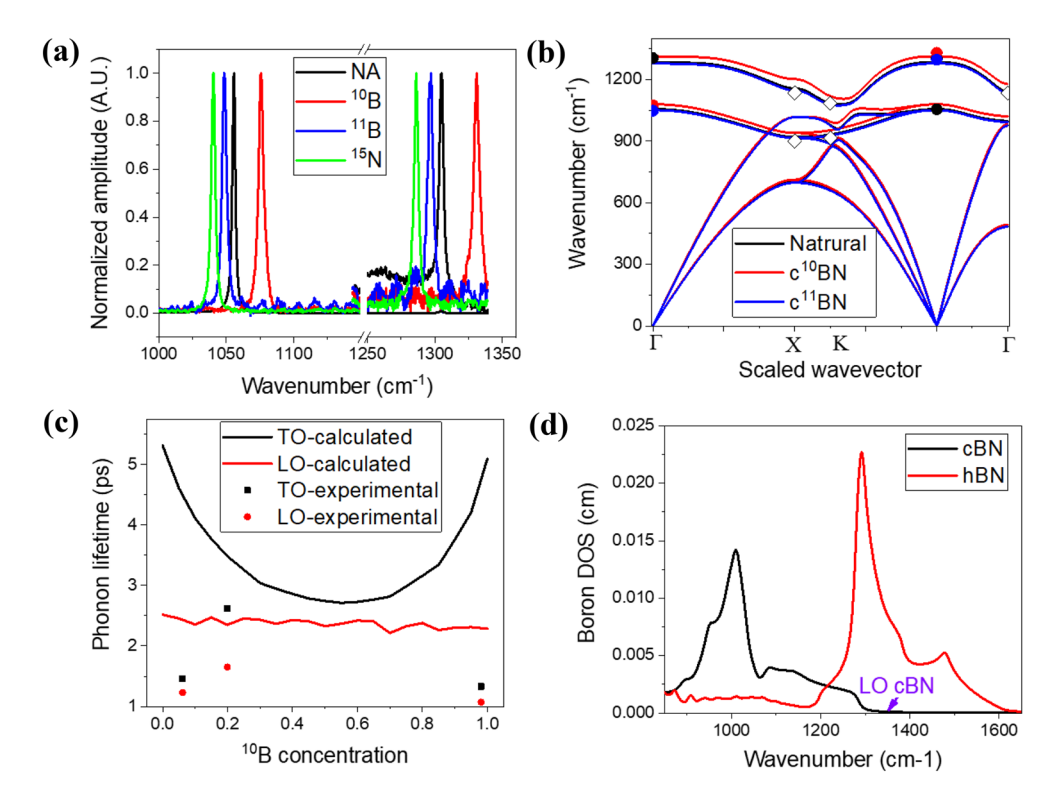


Figure 2: Phonon properties of cBN. (a) Raman spectra of different isotope enriched cBN with the baseline flattened. NA stands for natural abundant here. (b) Calculated phonon dispersion for cBN with natural isotope concentrations (solid black curves), pure ¹⁰B (solid red curves), and pure ¹¹B (solid blue curves). Solid circle symbols are Raman measurements from this work, while hollow diamonds are second-order Raman measurements from Ref. [42]. (c) Measured (symbols) and calculated (curves) phonon lifetimes of TO (black) and LO (red) Raman-active phonons in cBN with different ¹⁰B concentrations. The difference between calculated and experimental lifetimes is attributed to crystal impurities. (d) Partial phonon DOS (see text below Eq. 3) for boron vibrations (boron DOS) in cBN (black curve) and hBN (red curve).

TABLE 2: Phonon properties of cBN extracted from Raman spectra.

cBN	Peak [cm ⁻¹]	± Peak	FWHM [cm ⁻¹]	± FWHM	τ [ps]	Peak [cm ⁻¹]	Isotope ratio
c ¹⁰ BN	1075.9	0.5	3.97	0.03	1.33	1079.3	88%
	1330.9	0.5	4.95	0.11	1.07	1334.4	91%
c ¹¹ BN	1048.6	0.5	3.61	0.04	1.46	1050.3	>99%
	1296.7	0.5	4.32	0.06	1.23	1298.7	>99%
cB ¹⁵ N	1040.4	0.5	2.98	0.01	1.78	1040.4	98%
	1286.2	0.5	3.39	0.05	1.56	1286.3	97%
Natural cBN	1056.7	0.5	2.02	0.01	2.62	N/A	N/A
	1304.8	0.5	3.22	0.02	1.65	N/A	N/A

The dispersion can be used to deduce the phonon lifetimes limited by anharmonic three-phonon [43, 44] and phononisotope scatterings [45–47] (see SI) in cBN with different isotope concentrations. The resulting lifetimes provide a means of assessing the intrinsic phonon lifetimes expected with refined synthesis. Similar to our previous calculations for hBN [4], the calculated Raman-active TO phonon lifetimes are predicted to nearly double when transitioning from a 50/50 randomized mixture of boron isotopes to isotopically pure cBN (Fig. 2c). On the other hand, the calculated LO phonon lifetimes are found to be nominally insensitive to isotope variation. Note that the

phonon frequency shift will slightly influence the intrinsic three-phonon scattering, which makes the TO (LO) lifetimes of $c^{10}BN \sim 4\%$ ($\sim 9\%$) smaller than that of $c^{11}BN$. The calculations discussed above are performed with three-phonon scattering. Including four-phonon scattering gives slightly lower TO lifetimes ($\sim 4-8\%$), while the influence is negligible for LO lifetimes (further discussion in SI).

To further understand the disorder-limited lifetimes, we examine how various parameters influence phonon-isotope scattering. Quantum perturbation theory gives phonon-isotope scattering for a binary cubic crystal [45–47]:



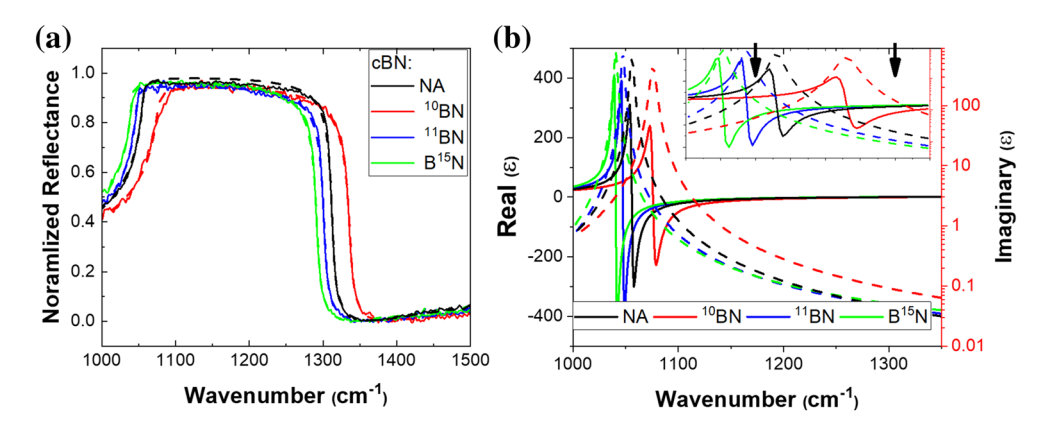


Figure 3: Dielectric function fitting of cBN. (a) Fitted and experimental FTIR reflectance of different isotopically enriched cBN. While experimental reflectance is shown as solid curves, fitted reflectance is shown as dashed curves; (b) Dielectric function of different isotopically enriched cBN. Real part of permittivity is plotted with solid curves, while the imaginary part is plotted with dashed curves. Inset is from 1030 to 1100 cm⁻¹ to highlight the shifted TO frequencies, with arrows highlighting the two vibrational frequencies of CO stretching mode. NA stands for naturally abundant cBN in the figure.

$$1/\tau_{\vec{q}j}^{ph-iso} = \frac{\pi V_{cell}}{6} \omega_{\vec{q}j}^2 \sum_{k} g_k |\hat{\epsilon}_{\vec{q}jk}|^2 D_k (\omega_{\vec{q}j})$$
 (3)

where V_{cell} is the volume of a unit cell of the crystal, and $\widehat{\epsilon}_{\bar{q}jk}$ is the eigenvector of the kth atom vibrations for phonon mode \bar{q} j. For the Raman modes considered here, $q\approx 0$ and j represents TO or LO polarizations. $D_k(\omega)=\sum_{\bar{q}j}\left|\hat{\epsilon}_{\bar{q}jk}\right|^2\delta(\omega-\omega_{\bar{q}j})$ are the partial phonon density of states (DOS) for the kth atom, calculated here with a tetrahedron method [48]. According to Eq. 3, both the higher phonon frequency $(\omega_{\bar{q}j})$ and larger DOS of hBN gives stronger phonon-isotope scattering rates compared with cBN (Fig. 2d). Thus, the lifetimes of hBN are predicted to be more sensitive to isotopic variance: the predicted maximum lifetimes of isotopically enriched hBN [4] (\sim 8 ps) exceed those of cBN (\sim 5 ps), while the calculated lifetimes of natural cBN (3.48 ps) far exceed that of natural hBN⁴ (0.86 ps). Additionally, the DOS vanishes for the cBN LO phonons resulting in lifetimes not influenced by isotope variations (Fig. 2c).

Based on the first-principles calculations described above, we attribute the observed broadening of isotopically enriched cBN to extrinsic defects and increases in the impurity density rather than the result of intrinsic properties. This interpretation is also supported by the yellow color and an increased level of visible photoluminescence for the isotopically enriched cBN (Fig. S1 and S2), both of which are associated with higher carbon and oxygen impurity concentrations [27, 49]. It should be mentioned that the growth technique for controlling the isotopic concentration of cBN is a very recent development, which is entirely different from the traditional process using growth solvent (see SI) [49]. As such, further synthesis developments are expected, potentially offering high-quality isotopically enriched cBN samples with phonon lifetimes approaching theoretical limits, as observed in natural cBN (Fig. 2c). Despite the broadening

caused by defects and impurities, the optic phonon lifetimes still remain over 1.3 ps for all the cBN samples investigated, which is comparable to the best reported lifetimes for isotopically enriched hBN (1.7 ps) [4]. As such, it is fair to claim that isotopic enrichment of cBN, even with such presumed increases in defect densities, still offers a method to tune the RB without compromising optical loss to unacceptable levels.

Leveraging the information derived thus far, we conclude by deducing the dielectric function of each isotopic variety of cBN probed in an effort to enable predictions of the optical response. The complex dielectric function of cBN was derived by modeling the FTIR reflection spectra shown in Fig. 3a using a single Lorentzian oscillator [20] [Eq. 4] of the dielectric tensor components under the TOLO formalism:

$$\varepsilon(\omega) = \varepsilon_{\infty} \frac{\omega_{LO}^2 - \omega^2 - i\gamma_{LO}\omega}{\omega_{TO}^2 - \omega^2 - i\gamma_{TO}\omega} \tag{4}$$

where ε_{∞} is the high-frequency dielectric permittivity, ω_{TO}/ω_{LO} are the frequencies of the TO/LO zone-center optic phonons, and γ_{TO}/γ_{LO} are the corresponding damping rates. The initial guesses for ω_{TO}/ω_{LO} were taken from our Raman data and those reported in the literature [20], with the final values extracted via least-square fitting of the FTIR reflectance data within the WVase software (J.A. Woollam Inc). The final phonon energies derived from the fits to the FTIR spectra are within 5 cm⁻¹ of those values measured with Raman spectroscopy. As the shape of cBN crystals offers multiple non-parallel facets (Fig. S2), the reflectance spectra outside of the RB, where increased transmission is observed, could not be accurately fit. Thus, this "out of band" spectral region was only used to estimate the value of ε_{∞} , serving as the initial values employed to fit the dielectric function of cBN in its RB region between ~ 1000 cm⁻¹ and 1500 cm⁻¹. Based on the experimental configuration used here (25° incident



angle), the reflectance maximum was determined to reach as high as 99% according to transfer matrix calculations, and thus, was used as the maximum reflectance for our fitting analysis. A summary of the resultant fitting parameters is provided in Table 3, with the fits exhibiting good quantitative agreement with the FTIR reflectance data, as illustrated in Fig. 3a. Values for peak energies and lifetimes are comparable between those derived from FTIR and Raman.

To provide a straightforward interpretation of dielectric function changes due to isotopic engineering, we plot the fitted dielectric functions of the various isotopically enriched cBN crystals in Fig. 3b. Because of the dependence ω_{TO} on the isotopic composition, the peaks in the imaginary part of the dielectric function appear at different frequencies for cBN with varying enrichment. This allows tuning the dielectric function over a given spectral range to match a particular vibration of interest. For instance, SEIRA detection of ethyl alcohol [50] requires matching the RB with one of the vibrational frequencies of the CO stretching mode (1090 cm⁻¹). Although this can be realized with natural cBN, the proximity of the CO stretching mode to the TO phonon implies high optical loss (i.e., $Im(\varepsilon)$ is large). By transitioning to $cB^{15}N$, the TO phonon is spectrally red-shifted by 15 cm⁻¹ resulting in an approximate halving of the imaginary part at the CO vibrational frequency (1090 cm⁻¹) from 1.9 (natural cBN) to 0.8 (cB15N), despite the higher quality of the naturally abundant crystals discussed here. Additionally, for molecules featuring vibrational resonances in the spectral range between 1040 and 1060 cm⁻¹, such as CO stretch in ethyl alcohol [50] at 1050 cm⁻¹, SEIRA cannot be employed with either naturally abundant cBN or hBN. Isotopic enrichment, however, makes these vibrations spectrally accessible, thereby extending the applicability of PhP-based approaches to molecular sensing.

While this work stresses that phonon frequencies and lifetimes can be modified via isotopic engineering, other strategies, such as dynamic intercalation and applying strains, can lead to similar outcomes. Although isotopic engineering does not provide a dynamic solution, it can be applied to all phonon material systems without introducing loss, as shown in Table 4. It should be noted that the frequency shift is related to the atomic mass and crystal structures.

Conclusions

Using isotopic engineering, the RBs of both cBN and hBN can be spectrally tuned by 35 cm⁻¹, and PhPs supported by BN allotropes are extended by 70 cm⁻¹, which covers a broad extent of the molecular-fingerprint region of the IR-spectrum. This offers significant opportunities in spectral tuning of the dielectric function for specific applications. While the phonon lifetimes of isotopically enriched hBN increase with isotopic enrichment, the opposite is observed here for cBN owing to extrinsic defects present in the material. First-principles calculations demonstrate that further refinement of synthesis should result in appreciable increases in the phonon lifetimes. Taken in aggregate, the results underscore the utility of isotopic engineering for tuning the optic phonons, thereby highlighting a path for more sensitive SEIRA detection [12], and the realization of narrow-band IR sources in frequency ranges that are otherwise inaccessible with PhP-supporting materials [18, 19, 53]. Furthermore, the engineering of optical phonons potentially facilitates the understanding and manipulating of phonon sidebands in single photon emitters [31].

TABLE 3: Fitting parameters of different cBN from FTIR data, and uncertainties from fitting are included.

cBN	ε _∞	±ε _∞	Peak [cm ⁻¹]	± Peak	γ [cm ⁻¹]	±γ	τ [ps]
			r cur [ciri		y term 1		. [b2]
c ¹⁰ BN	4.26	0.03	1074.7	0.3	11.4	0.3	0.46
			1328.5	0.2	7.9	0.1	0.67
c ¹¹ BN	4.49	0.03	1048.2	0.3	4.0	0.3	1.33
			1295.0	0.2	5.9	0.1	0.90
$cB^{15}N$	4.48	0.02	1040.7	0.2	4.0	0.1	1.33
			1284.2	0.1	5.65	0.08	0.94
Natural cBN	4.19	0.002	1055.4	0.1	2.25	0.08	2.36
			1306.2	0.1	5.23	0.05	1.01

TABLE 4: Comparison among different strategies to engineer phonon frequencies.

Strategy	Materials	Frequency shift (%)	Loss introduced?	Dynamic tuning?	Universal?	
Isotopic engineering	cBN and hBN	3.3	No	No	Yes	
Ionic intercalation [51]	α - V_2O_5	3.5	Yes	Yes	No	
Strain [52]	hBN	0.3%	Not discussed	Potentially yes	Yes	



Methods

Material growth

cBN crystals with naturally abundant boron isotope distributions were grown by a conventional temperature gradient method under high pressure. Commercial hBN with natural isotope abundances as starting material was placed with a barium-based solvent in a Molybdenum (Mo) capsule where the bottom cooler end is solvent. Because of the temperature gradient in the Mo capsule in high-pressure assembly, dissolved sources of hBN crystals were precipitated as cBN at the cooler end of the capsule as described in detail in Ref. [54]. By controlling pressure and temperature for the crystal growth, cBN and/or hBN crystals can be obtained (Ref [49].).

Hot-pressed hBN disks (Denka Co. Ltd., Japan, type N1) and powder hBN (Denka Co. Ltd., Japan, type GP) were used as the natural BN source, and they were heated at 2100 °C for 2 h in a nitrogen flow to remove residual oxygen. Single crystals of relatively large size (\sim 500 μ m) with almost no color are often harvested (Fig. S1a) [49, 54]. In comparison, the boron isotope-controlled crystals were obtained using the metathesis reaction below between NaBH4 (KATCHEM spol.s.r.o. Na 10 BH₄ with 99.7% 10 B, and Na 11 BH₄ with 99.8% 11 B) and NH₄Cl (Wako Chemicals, >99.0%) under high pressure. For the 15 N enrichment, 15 NH₄Cl (Shoko Science Co Ltd, 99.0%) was used. The reaction is

$$Na^{m}BH_{4} + {}^{n}NH_{4}Cl = {}^{m}B^{n}N + NaCl + 2H_{2},$$

where ${}^{\rm m}{\rm B}$ denotes either ${}^{10}{\rm B}$ or ${}^{11}{\rm B}$. By choosing the mixing ratio of Na ${}^{10}{\rm BH_4}$ and Na ${}^{11}{\rm BH_4}$, the ${}^{10}{\rm B}$ and ${}^{11}{\rm B}$ content in the resulting cBN crystals can be controlled. ${}^{\rm n}{\rm N}$ denotes either ${}^{14}{\rm N}$ or ${}^{15}{\rm N}$ as well. Briefly, starting chemicals as mentioned above were assembled in Mo capsules in a dry nitrogen purged glovebox where humidity and oxygen were less than 1 ppm. Then the capsules were treated at a pressure of 6.0 GPa and a temperature of 1500 ${}^{\circ}{\rm C}$ for 3 h. After releasing the pressure, the Mo capsules were dissolved by hot aqua regia to recover the grown cBN crystals.

The metathesis reaction-based growth of cBN crystals is a recent progress and our report here marks the first success. It is totally different from processes using growth solvent [49, 54]. More studies will be pursued and details will be described in a separate paper.

Fourier transform infrared spectroscopy

FTIR reflectance was measured using a Bruker Hyperion 2000 FTIR Microscope coupled to a Bruker Vertex 70v Fourier transform infrared (FTIR) spectrometer with a spectral resolution of 2 cm⁻¹. The microscope was equipped with a reflective $36 \times Cassegrain$ objective (NA = 0.17), and a liquid-nitrogen cooled mercury cadmium telluride (MCT) detector. The use of a $36 \times objective$ enables us to optimize the signal over a 30 μ m by 30 μ m

area, so the influence of surface roughness and the non-planar curvature of the sample surface are minimized. The reflectance spectra were referenced to a gold mirror.

Raman spectroscopy

Raman spectra were acquired with a WiTec alpha300R Raman microscope equipped with a 532 nm laser that was focused to a nominally diffraction-limited spot upon the sample using a $20 \times \text{objective}$ (NA = 0.45). The spectral accuracy was calibrated using ASTM E1840-96 resulting in a spectral accuracy of < 0.5 cm⁻¹ from day to day. Precision within a given measurement was more than $10 \times \text{less}$ than this value. To reduce random error and to analyze the uniformity of BN phonon behavior, we acquired 30–90 spectra for each sample at different locations and then fit each acquisition separately. Reported values are the mean values and 95% confidence intervals for a given value. For peak positions, uncertainty is dominated by Type B uncertainty related to absolute calibration of the Raman spectrometer rather than variation within the sample itself (i.e., Type A uncertainty).

Linewidths (i.e., FWHM) of a given Raman mode were quantified by fitting the Raman response to a Voigt profile and then deconvoluting the spectrometer response function using Posener's tables whereupon the lifetime was deduced by employing the energy-time uncertainty relationship [30]. The spectrometer response function was found to be 1.05 cm⁻¹, which is less than half that of the narrowest hBN linewidth.

First-principles calculations

Calculations of the phonon dispersions and Raman frequencies $(\omega_{\vec{q}i}, \text{ with } \vec{q} \text{ being the phonon wavevector and } j \text{ being }$ the polarization) were derived from harmonic interatomic force constants (IFCs) determined within the framework of density functional perturbation theory [40, 55, 56] and the local density approximation using the Quantum Espresso software suite [41, 57]. These included the effects of long-range Coulomb interactions (LO/TO splitting) [40] via calculated Born charges (± 1.89e) and the high-frequency dielectric tensor (4.66 on the diagonal elements, zero for off-diagonal elements). Structural relaxation via energy minimization using Perdew-Zunger exchange correlations [58], norm-conserving pseudopotentials (Bachelet-Hamann-Schlüter [59] for boron, von Barth-Car [60] for nitrogen), $6 \times 6 \times 6$ electronic integration grid, and plane wave energy cutoff of 100 Ry give a lattice parameter a = 3.59 Å. The harmonic IFCs $(\Phi_{\alpha\beta}^{lk,l'k'})$ [43, 44] were determined on a 6×6 x6 reciprocal space integration grid. Here, $\Phi_{\alpha\beta}^{lk,l'k'}$ are the spring constants connecting the kthatom in the lth unit cell along the αth Cartesian direction with the k'th in the l'th unit cell in the βth direction.

Calculated isotope-dependent Raman lifetimes were determined via quantum perturbation theory calculations of



three-phonon [43, 44], four-phonon [43, 61, 62], and phonon-isotope scattering [45–47]. Anharmonic IFCs (third- and fourth-order) were calculated from numerical derivatives of interatomic forces determined from atomic perturbations in 216-atom supercells with Γ -point-only calculations, otherwise using similar details described above. Interaction cutoff distances were defined as 3.05 Å (3rd nearest neighbor shell) and 2.7 Å (2nd nearest neighbor shell) for third- and fourth-order IFCs, respectively. The form of the three-phonon [63, 64] and four-phonon [61, 62] scattering rates have been described previously.

Acknowledgments

M. H. and J. D. C. gratefully acknowledge support for this work by Office of Naval Research Grant N00014-18-12107. L. L. acknowledges support for theory and numerical calculations from the US Department of Energy, Office of Science, Office of Basic Energy Sciences, Material Sciences and Engineering Division. J. M. was supported by the National Science Foundation, Division of Materials Research under grant number 1904793. Computational resources were provided by the National Energy Research Scientific Computing Center (NERSC), a DOE Office of Science User Facility supported by the Office of Science of the US Department of Energy under Contract No. DE-AC02-05CH11231. A. McDonald is recognized for his work in supporting Raman spectroscopy efforts. This work was undertaken, in part, at the Center for Integrated Nanotechnologies, an Office of Science User Facility operated for the US Department of Energy (DOE) Office of Science. Sandia National Laboratories is a multimission laboratory managed and operated by National Technology & Engineering Solutions of Sandia, LLC, a wholly owned subsidiary of Honeywell International, Inc., for the US DOE's National Nuclear Security Administration under Contract No. DE-NA-0003525. K.W. and T.T. acknowledge support from the Elemental Strategy Initiative conducted by the MEXT, Japan, Grant Number JPMXP0112101001 and Grant Number JP20H00354. T.G.F. was supported by Vanderbilt University through J. D. C's startup package.

Declarations

Conflict of interest The authors declare that there is no conflict of interest.

Data availability

The data generated during and/or analyzed during the current study are available from the corresponding author on reasonable request.

Supplementary Information

The online version contains supplementary material available at https://doi.org/10.1557/s43578-021-00426-9.

References

- Z. Liu et al., Far-field optical hyperlens magnifying sub-diffraction-limited objects. Science 315, 1686–1686 (2017)
- T. Nagatsuma et al., Advances in terahertz communications accelerated by photonics. Nat. Photonics 10, 371 (2016)
- L.V. Brown et al., Fan-shaped gold nanoantennas above reflective substrates for surface-enhanced infrared absorption (SEIRA).
 Nano Lett. 15, 1272–1280 (2015)
- 4. A.J. Giles et al., Ultralow-loss polaritons in isotopically pure boron nitride. Nat. Mater. 17, 134 (2018)
- S. A Maier, in *Plasmonics: fundamentals and applications*. (Springer Science & Business Media, 2007)
- A.-K.U. Michel et al., Using low-loss phase-change materials for mid-infrared antenna resonance tuning. Nano Lett. 13, 3470–3475 (2013)
- J.D. Caldwell et al., Low-loss, extreme subdiffraction photon confinement via silicon carbide localized surface phonon polariton resonators. Nano Lett. 13, 3690–3697 (2013)
- T. Wang et al., Optical properties of single infrared resonant circular microcavities for surface phonon polaritons. Nano Lett. 13, 5051–5055 (2013)
- 9. P. Li et al., Infrared hyperbolic metasurface based on nanostructured van der Waals materials. Science **359**, 892–896 (2018)
- O. Dominguez, et al., Monochromatic multimode antennas on epsilon-near-zero materials. Adv. Opti. Mater. 1800826 (2019)
- Y. Chen et al., Spectral tuning of localized surface phonon polariton resonators for low-loss mid-IR applications. ACS Photonics 1, 718–724 (2014)
- M. Autore, et al., Boron nitride nanoresonators for phononenhanced molecular vibrational spectroscopy at the strong coupling limit. Light Sci. Amp Appl. 7, 17172. https://doi.org/10. 1038/lsa.2017.172. https://www.nature.com/articles/lsa2017172# supplementary-information (2018)
- 13. P. Sohr et al., Far-field thermal emission from a semiconductor hyperbolic metamaterial. Opt. Lett. **44**, 1138–1141 (2019)
- 14. T.G. Folland et al., Vibrational Coupling to Epsilon-Near-Zero Waveguide Modes. ACS Photonics 7, 614–621 (2020)
- M.S. Anderson, Surface enhanced infrared absorption by coupling phonon and plasma resonance. Appl. Phys. Lett. 87, 144102 (2005)
- R. Berte et al., Sub-nanometer thin oxide film sensing with localized surface phonon polaritons. ACS Photonics 5, 2807–2815 (2018)
- 17. J.-J. Greffet et al., Coherent emission of light by thermal sources. Nature **416**, 61 (2002)



- 18. J.A. Schuller et al., Optical antenna thermal emitters. Nat. Photonics **3**, 658 (2009)
- T. Wang et al., Phonon-polaritonic bowtie nanoantennas: controlling infrared thermal radiation at the nanoscale. ACS Photonics 4, 1753–1760 (2017)
- I. Chatzakis et al., Strong confinement of optical fields using localized surface phonon polaritons in cubic boron nitride. Opt. Lett. 43, 2177–2180 (2018)
- M. He et al., Guided mid-IR and near-IR light within a hybrid hyperbolic-material/silicon waveguide heterostructure. Adv. Mater. 33, 2004305 (2021)
- I.-H. Lee et al., Image polaritons in boron nitride for extreme polariton confinement with low losses. Nat. Commun. 11, 1–8 (2020)
- T.G. Folland et al., Reconfigurable infrared hyperbolic metasurfaces using phase change materials. Nat. Commun. 9, 1–7 (2018)
- 24. K. Chaudhary et al., Polariton nanophotonics using phasechange materials. Nat. Commun. **10**, 1–6 (2019)
- M. He et al., Ultrahigh-resolution, label-free hyperlens imaging in the Mid-IR. Nano Lett. 21, 7921–7928 (2021). https://doi.org/ 10.1021/acs.nanolett.1c01808
- Y. Kubota et al., Synthesis of cubic and hexagonal boron nitrides by using Ni solvent under high pressure. Jpn. J. Appl. Phys. 46, 311 (2007)
- 27. T. Taniguchi et al., Defect characterization of cBN single crystals grown under HP/HT. Phys. Status Solidi **201**, 2573–2577 (2004)
- R. Cuscó et al., Effects of isotopic substitution on the phonons of van der Waals crystals: the case of hexagonal boron nitride. J J. Phys. D Appl. Phys. 52, 303001 (2019)
- 29. P.-F. Lory et al., Direct measurement of individual phonon lifetimes in the clathrate compound Ba 7.81 Ge 40.67 Au 5.33. Nat. Commun. **8**, 491 (2017)
- T. Beechem, S. Graham, Temperature and doping dependence of phonon lifetimes and decay pathways in GaN. J. Appl. Phys. 103, 093507 (2008)
- J.D. Caldwell et al., Photonics with hexagonal boron nitride. Nat. Rev. Mater. 4, 552–567 (2019)
- S. Dai et al., Subdiffractional focusing and guiding of polaritonic rays in a natural hyperbolic material. Nat. Commun. 6, 6963 (2015). https://doi.org/10.1038/ncomms7963
- P. Li et al., Hyperbolic phonon-polaritons in boron nitride for near-field optical imaging and focusing. Nat. Commun. 6, 7507 (2015)
- I. Aharonovich et al., Solid-state single-photon emitters. Nat. Photonics 10, 631 (2016)
- 35. T.T. Tran et al., Quantum emission from hexagonal boron nitride monolayers. Nat. Nanotechnol. 11, 37 (2016)
- N. Chejanovsky et al., Structural attributes and photodynamics of visible spectrum quantum emitters in hexagonal boron nitride. Nano Lett. 16, 7037–7045 (2016)

- G. Cassabois et al., Hexagonal boron nitride is an indirect bandgap semiconductor. Nat. Photonics 10, 262 (2016)
- T. Vuong et al., Deep ultraviolet emission in hexagonal boron nitride grown by high-temperature molecular beam epitaxy. 2D Materials 4, 021023 (2017)
- H. Jiang et al., Hexagonal boron nitride for deep ultraviolet photonic devices. Semicond. Sci. 29, 084003 (2014)
- S. Baroni et al., Phonons and related crystal properties from density-functional perturbation theory. Rev. Mod. Phys. 73, 515 (2001)
- 41. P. Giannozzi et al., QUANTUM ESPRESSO: a modular and open-source software project for quantum simulations of materials. J. Phys. Conds. Matter. 21, 395502 (2009)
- 42. S. Reich et al., Resonant Raman scattering in cubic and hexagonal boron nitride. Phys. Rev. B **71**, 205201 (2005). https://doi.org/10.1103/PhysRevB.71.205201
- 43. J. Ziman, Electrons and Phonons: The Theory of Transport Phenomena in Solids (Clarendon, Oxford, 1960)
- 44. G.P. Srivastava, in The physics of phonons. (Routledge, 2019)
- 45. S.-I. Tamura, Isotope scattering of dispersive phonons in Ge. Phys. Rev. B **27**, 858 (1983)
- S.-I. Tamura, Isotope scattering of large-wave-vector phonons in GaAs and InSb: deformation-dipole and overlap-shell models. Phys. Rev. B 30, 849 (1984)
- 47. L. Lindsay et al., Phonon-isotope scattering and thermal conductivity in materials with a large isotope effect: a first-principles study. Phys. Rev. B **88**, 144306 (2013)
- 48. G. Lehmann, M. Taut, On the numerical calculation of the density of states and related properties. Phys. Status Solidi (b) **54**, 469–477 (1972)
- T. Taniguchi, K. Watanabe, Synthesis of high-purity boron nitride single crystals under high pressure by using Ba–BN solvent. J. Cryst. Growth 303, 525–529 (2007)
- Spectral database for organic compounds SDBS free site organized by National Institute of Advanced Industrial Science and Technology (AIST), Japan, http://riodb01.ibase.aist.go.jp/sdbs/cgi-bin/creindex.cgi
- J. Taboada-Gutiérrez, et al., Broad spectral tuning of ultra-lowloss polaritons in a van der Waals crystal by intercalation. Nat. Mater. 1–5 (2020)
- 52. B. Lyu, et al., Phonon polariton-assisted infrared nanoimaging of local strain in hexagonal boron nitride. Nano Lett. (2019)
- G. Lu et al., Narrowband polaritonic thermal emitters driven by waste heat. ACS Omega (2020). https://doi.org/10.1021/acsom ega.0c00600
- T. Taniguchi, S. Yamaoka, Spontaneous nucleation of cubic boron nitride single crystal by temperature gradient method under high pressure. J. Cryst. Growth 222, 549–557 (2001)
- P. Hohenberg, W. Kohn, Inhomogeneous electron gas. Phys. Rev. 136, B864 (1964)



- W. Kohn, L.J. Sham, Self-consistent equations including exchange and correlation effects. Phys. Rev. 140, A1133 (1965)
- 57. QUANTUM ESPRESSO. http://www.quantum-espresso.org.
- J.P. Perdew, A. Zunger, Self-interaction correction to densityfunctional approximations for many-electron systems. Phys. Rev. B 23, 5048 (1981)
- 59. G. Bachelet et al., Pseudopotentials that work: From H to Pu. Phys. Rev. B **26**, 4199 (1982)
- 60. A. Dal Corso et al., Ab initio calculation of phonon dispersions in II-VI semiconductors. Phys. Rev. B 47, 3588 (1993)
- T. Feng, X. Ruan, Quantum mechanical prediction of four-phonon scattering rates and reduced thermal conductivity of solids. Phys. Rev. B 93, 045202 (2016)
- 62. T. Feng et al., Four-phonon scattering significantly reduces intrinsic thermal conductivity of solids. Phys. Rev. B **96**, 161201 (2017)
- L. Lindsay et al., Thermal conductivity and large isotope effect in GaN from first principles. Phys. Rev. Lett. 109, 095901 (2012)
- 64. L. Lindsay et al., Ab initio thermal transport in compound semiconductors. Phys. Rev. B **87**, 165201 (2013)